

A New Consistency Test for the Λ CDM Model using Radial and Transverse BAO Measurements

XING-HAN A. ZHAO¹ AND ZHENG CAI²

¹*The International Division of the Second High School Attached to Beijing Normal University, Beijing 100192, P.R.China*

²*Department of Astronomy, Tsinghua University, Beijing 100084, P.R.China*

ABSTRACT

We present a calibration-free consistency test of spatially flat Λ CDM based on baryon acoustic oscillation (BAO) distance measurements. The method forms ratios of BAO distances including the Hubble distance, the comoving angular diameter distance, and the volume-averaged distance, so that the sound horizon scale cancels, and then maps each observed ratio to an effective flat- Λ CDM matter density parameter, Ω_M^Λ , defined as the value of Ω_M that reproduces the measured ratio within Λ CDM. Flat Λ CDM predicts that Ω_M^Λ should be independent of redshift and of the particular ratio used. For ratios involving the integrated distances, we associate them with well-defined effective line-of-sight redshift intervals based on the integral mean value theorem. We apply the test to BAO measurements from the Dark Energy Spectroscopic Instrument (DESI) Data Release 1 and Data Release 2, propagating the full published BAO covariance matrices into all derived ratios and Ω_M^Λ constraints. Within current uncertainties, the inferred Ω_M^Λ values are broadly consistent with a redshift-independent constant, providing an internal consistency check of flat Λ CDM that can be strengthened straightforwardly as BAO measurements improve.

Keywords: cosmological parameters — large-scale structure of Universe — baryon acoustic oscillations

1. INTRODUCTION

The discovery that the cosmic expansion is accelerating (A. G. Riess et al. 1998; S. Perlmutter et al. 1999) has made the physical origin of dark energy one of the central problems in modern cosmology. In the standard picture, cosmic acceleration is attributed to a cosmological constant (vacuum energy) (S. Weinberg 1989; S. M. Carroll 2001) or to a dynamical component (B. Ratra & P. J. E. Peebles 1988; R. R. Caldwell et al. 1998). At the same time, the spatially-flat Λ CDM model has achieved remarkable empirical success in describing a broad set of observations, including the temperature anisotropies of the cosmic microwave background (CMB), from the first detection by COBE to subsequent measurements of the acoustic peak structure (G. F. Smoot et al. 1992; C. L. Bennett et al. 1996; P. de Bernardis et al. 2000; N. W. Halverson et al. 2002), as well as the observed clustering and growth of large-scale structure (P. J. E. Peebles 1980). It therefore remains essential to develop robust, low-assumption consistency tests that can expose subtle

departures from flat Λ CDM or reveal residual observational systematics.

Baryon acoustic oscillations (BAO) provide one of the most robust late-time geometric probes. The BAO feature was first robustly detected in galaxy redshift surveys in 2005 using the Sloan Digital Sky Survey and the Two-degree Field Galaxy Redshift Survey (2dFGRS) (D. J. Eisenstein et al. 2005; S. Cole et al. 2005), and it has since become a standard ruler exploited by many surveys (S. Alam et al. 2021). Modern spectroscopic surveys now deliver high-precision BAO constraints over a broad redshift range, including recent measurements from the Dark Energy Spectroscopic Instrument (DESI) (A. G. Adame et al. 2025a; M. Abdul Karim et al. 2025). A practical complication is that BAO are primarily measured as *relative* distances in units of the sound horizon at the drag epoch, and different BAO statistics constrain different combinations of line-of-sight and transverse distances. This can make it non-trivial to apply popular $H(z)$ -based null diagnostics to the full set of BAO observables in a unified way.

A widely-used diagnostic for testing flat Λ CDM is the Om statistic (V. Sahni et al. 2008; C. Zunckel & C. Clarkson 2008; V. Sahni et al. 2014; A. Shafieloo et al.

2012), which is constructed to be constant in redshift for a flat Λ CDM cosmology and to vary when the expansion history deviates from this model. In practice, however, transverse BAO constraints involve integrated distance information, so straightforward applications of Om naturally favor local expansion-rate measurements or require additional steps and assumptions to incorporate transverse BAO consistently.

In this work we devise a simple, ratio-based BAO consistency test that can simultaneously exploit radial and transverse BAO information while remaining insensitive to the absolute BAO scale. The basic idea is to form appropriately chosen ratios of BAO distance measurements so that the sound horizon (and overall calibration) cancels, and then ask whether these ratios are mutually consistent with a single flat Λ CDM matter density parameter. Each observed ratio can be mapped to an effective Λ CDM matter density, Ω_M^Λ , and the redshift-independence of Ω_M^Λ across different ratios and redshift pairs provides a direct null test of flat Λ CDM. To incorporate transverse and isotropic BAO information in a transparent manner, we use a redshift-matching strategy based on the integral mean value theorem (W. Rudin 1976) to relate integrated BAO distances to an effective line-of-sight distance over a well-defined redshift interval.

This paper is organized as follows. In Section 2 we describe the construction of the ratio diagnostics, the mapping to Ω_M^Λ , the redshift-matching procedure, and the data sets used. Section 3 presents the results for DESI DR1 and DR2 BAO measurements. We summarize and discuss implications in Section 4, and provide additional details of the redshift-matching procedure in an appendix.

2. METHODOLOGY AND DATA

2.1. From the Om diagnostic to BAO ratio tests

The Om diagnostic (V. Sahni et al. 2008; C. Zunckel & C. Clarkson 2008) is a widely-used null test of flat Λ CDM based on the expansion rate,

$$Om(z) \equiv \frac{h^2(z) - 1}{(1+z)^3 - 1}, \quad h(z) \equiv H(z)/H_0, \quad (1)$$

which is constant and equal to the present-day matter density parameter Ω_M in a spatially flat Λ CDM universe. To reduce sensitivity to the absolute calibration of H_0 , a two-point version was proposed (V. Sahni et al. 2014),

$$Om(z_i, z_j) = \frac{h^2(z_i) - h^2(z_j)}{(1+z_i)^3 - (1+z_j)^3}. \quad (2)$$

While these diagnostics are naturally suited to local measurements of $H(z)$, modern BAO analyses provide

a broader set of observables, including transverse (integrated) distances. We therefore construct ratio-based diagnostics from BAO distance measurements that (i) cancel the sound horizon scale r_d and (ii) can be applied uniformly to radial and transverse BAO.

We adopt the standard BAO distance definitions: the Hubble distance $D_H(z) \equiv c/H(z)$, the comoving angular diameter distance

$$D_M(z) = \int_0^z D_H(z') dz', \quad (3)$$

and the volume-averaged BAO distance

$$D_V(z) = [z D_M^2(z) D_H(z)]^{1/3}. \quad (4)$$

BAO constraints are commonly reported as D_H/r_d , D_M/r_d , or D_V/r_d , so appropriately chosen ratios of BAO distances are independent of the absolute BAO scale r_d (and, for our purposes, also independent of the overall normalization set by H_0).

2.2. Ratio diagnostics and the effective Λ CDM matter density Ω_M^Λ

Our null test is based on mapping each observed distance ratio to an *effective* matter density parameter in flat Λ CDM, denoted by Ω_M^Λ , defined as the value of Ω_M that reproduces the observed ratio within a flat Λ CDM prediction. If the Universe is described by flat Λ CDM, all ratios (and all redshift pairs) should yield a consistent, redshift-independent $\Omega_M^\Lambda = \Omega_M$. Any statistically significant redshift dependence of Ω_M^Λ indicates an inconsistency with flat Λ CDM (which could arise from dynamical dark energy, spatial curvature, modified gravity, or residual observational systematics).

2.2.1. Radial–radial test (R_{HH})

We first construct a purely radial ratio using D_H at two redshifts:

$$\frac{D_H(z_i)}{D_H(z_j)} \equiv R_{HH}(z_i, z_j) \xrightarrow{\Lambda} R_{HH}^\Lambda(z_i, z_j) \equiv \frac{D_H^\Lambda(z_i)}{D_H^\Lambda(z_j)}. \quad (5)$$

In a spatially flat Λ CDM model parameterized by Ω_M^Λ , the Hubble distance is

$$D_H^\Lambda(z) = \frac{c}{H_0 \sqrt{\Omega_M^\Lambda(1+z)^3 + (1-\Omega_M^\Lambda)}}. \quad (6)$$

Equating $R_{HH}(z_i, z_j) = R_{HH}^\Lambda(z_i, z_j)$ yields an analytic expression for Ω_M^Λ in terms of the observed ratio:

$$\Omega_M^\Lambda = \frac{1 - R_{HH}^2(z_i, z_j)}{R_{HH}^2(z_i, z_j) f(z_j) - f(z_i)}, \quad (7)$$

where $f(z) \equiv (1+z)^3 - 1$. Note that c and H_0 cancel out in the ratio and therefore do not affect the inferred Ω_M^Λ .

2.2.2. Radial-transverse test (R_{HM} ; diagonal)

We adopt the “diagonal” radial-transverse ratio,

$$R_{\text{HM}}(z) \equiv \frac{D_{\text{H}}(z)}{D_{\text{M}}(z)} \xrightarrow{\Lambda} R_{\text{HM}}^{\Lambda}(z; \Omega_{\text{M}}^{\Lambda}) \equiv \frac{D_{\text{H}}^{\Lambda}(z)}{D_{\text{M}}^{\Lambda}(z)}, \quad (8)$$

where $D_{\text{M}}^{\Lambda}(z) = \int_0^z D_{\text{H}}^{\Lambda}(z') dz'$ and $D_{\text{H}}^{\Lambda}(z)$ is given by Eq. (6). In practice we evaluate $R_{\text{HM}}(z)$ at the BAO redshift-bin centers z_i as $R_{\text{HM}}(z_i) = D_{\text{H}}(z_i)/D_{\text{M}}(z_i)$, constructed directly from the anisotropic BAO constraints ($D_{\text{H}}/r_{\text{d}}$, $D_{\text{M}}/r_{\text{d}}$) reported in the same redshift bin. This choice enables us to propagate the full DESI BAO covariance (including the correlation between D_{H} and D_{M} within each bin) into the derived R_{HM} and $\Omega_{\text{M}}^{\Lambda}$ constraints.

Although one can define a more general hybrid family

$$R_{\text{HM}}(z_i, z_j) \equiv \frac{D_{\text{H}}(z_i)}{D_{\text{M}}(z_j)}, \quad (9)$$

we do not pursue the full two-redshift set in this work. Once the radial-radial ratios $R_{\text{HH}}(z_i, z_j) = D_{\text{H}}(z_i)/D_{\text{H}}(z_j)$ are included, allowing $z_i \neq z_j$ in R_{HM} produces an overcomplete collection of tests that repeatedly reuses the same $D_{\text{H}}(z_i)$ measurements, leading to strong correlations among the inferred $\Omega_{\text{M}}^{\Lambda}$ values and complicating interpretation. We therefore restrict to the diagonal ratio in Eq. (8), which cleanly incorporates transverse information without duplicating the cross-redshift leverage already captured by R_{HH} .

Because $D_{\text{M}}^{\Lambda}(z)$ involves an integral, there is no closed-form inversion analogous to Eq. (7). We therefore determine $\Omega_{\text{M}}^{\Lambda}$ by numerically solving the one-dimensional equation $R_{\text{HM}}^{\Lambda}(z; \Omega_{\text{M}}^{\Lambda}) = R_{\text{HM}}(z)$ for $\Omega_{\text{M}}^{\Lambda} \in [0, 1]$.

2.2.3. Radial-isotropic test (R_{HV})

Similarly, we define a ratio between a radial distance and the volume-averaged distance:

$$\frac{D_{\text{H}}(z_i)}{D_{\text{V}}(z_j)} \equiv R_{\text{HV}}(z_i, z_j) \xrightarrow{\Lambda} R_{\text{HV}}^{\Lambda}(z_i, z_j) \equiv \frac{D_{\text{H}}^{\Lambda}(z_i)}{D_{\text{V}}^{\Lambda}(z_j)}, \quad (10)$$

where $D_{\text{V}}^{\Lambda}(z) = [z (D_{\text{M}}^{\Lambda}(z))^2 D_{\text{H}}^{\Lambda}(z)]^{1/3}$. As for R_{HM} , we infer $\Omega_{\text{M}}^{\Lambda}$ by numerically solving $R_{\text{HV}}^{\Lambda}(z_i, z_j; \Omega_{\text{M}}^{\Lambda}) = R_{\text{HV}}(z_i, z_j)$.

2.3. Effective-redshift interpretation and redshift ranges

The transverse and isotropic distances encode *integrated* information about $D_{\text{H}}(z)$. For interpretation and for visual comparisons, it is useful to associate D_{M} and D_{V} with an effective redshift at which they correspond to a local Hubble distance. By the integral mean value

theorem (W. Rudin 1976), there exists an intermediate redshift $z_c \in (0, z)$ such that

$$\begin{aligned} D_{\text{M}}(z) &= z D_{\text{H}}(z_c), \\ D_{\text{M}}^{\Lambda}(z) &= z D_{\text{H}}^{\Lambda}(z_c^{\Lambda}), \end{aligned} \quad (11)$$

where z_c^{Λ} is the corresponding intermediate redshift in a given Λ CDM model. Likewise, using Eq. (4) and Eq. (11), one can write

$$\begin{aligned} D_{\text{V}}(z) &= [z D_{\text{M}}^2(z) D_{\text{H}}(z)]^{1/3} \\ &= z [D_{\text{H}}^2(z_c) D_{\text{H}}(z)]^{1/3} \equiv z D_{\text{H}}(z_d), \end{aligned} \quad (12)$$

for some z_d satisfying $z_c < z_d < z$.

In practice, z_c and z_d are not directly observable and depend (weakly) on the assumed background model. To provide a conservative and transparent summary of which redshift interval each ratio probes, we report a *redshift range* for each test: for $R_{\text{HH}}(z_i, z_j)$ it is simply $[z_i, z_j]$; for $R_{\text{HM}}(z)$ it is $[z_c, z]$; and for $R_{\text{HV}}(z_i, z_j)$ it is $[z_d, z_i]$, where $z_d < z_j$. When needed, we bracket these intermediate-redshift mappings by scanning $\Omega_{\text{M}}^{\Lambda}$ over a broad prior range (we take $\Omega_{\text{M}}^{\Lambda} \in [0, 1]$) to obtain conservative bounds on z_c^{Λ} and z_d^{Λ} for quoting the corresponding interval. Additional details of the mapping are provided in the Appendix.

2.4. Converting D_{M} measurements into an effective D_{H} over a redshift interval

When D_{M} is measured at two redshifts $z_1 < z_2$, the difference

$$\begin{aligned} D_{\text{M}}(z_1, z_2) &\equiv D_{\text{M}}(z_2) - D_{\text{M}}(z_1) \\ &= \int_{z_1}^{z_2} D_{\text{H}}(z') dz' = (z_2 - z_1) D_{\text{H}}(z_*), \end{aligned} \quad (13)$$

for some $z_* \in (z_1, z_2)$ by the integral mean value theorem (W. Rudin 1976). This relation defines an *effective* Hubble distance $D_{\text{H}}(z_*) \equiv D_{\text{M}}(z_1, z_2)/(z_2 - z_1)$ associated with the redshift interval $[z_1, z_2]$. We use (z_1, z_2) to quantify the redshift range for this converted D_{H} in our figures and tables.

2.5. Data sets

We use BAO measurements from the Dark Energy Spectroscopic Instrument (DESI) Data Release 1 (DR1) (A. G. Adame et al. 2025a,b) and Data Release 2 (DR2) (M. Abdul Karim et al. 2025). The inputs are the published BAO constraints on $D_{\text{H}}/r_{\text{d}}$, $D_{\text{M}}/r_{\text{d}}$, and/or $D_{\text{V}}/r_{\text{d}}$ in each redshift bin, from which we form the ratios in Eqs. (5)–(10). Because our diagnostics are ratios of BAO distances, the sound horizon r_{d} cancels exactly. Throughout, we use the full DESI BAO covariance matrices provided with the data products, and propagate them into all derived ratios and $\Omega_{\text{M}}^{\Lambda}$ constraints.

2.6. Uncertainty propagation

We propagate measurement uncertainties using the *full* DESI BAO covariance matrices. For each data release we construct the BAO data vector (including all reported distance parameters across redshift bins) and its associated covariance matrix, and generate Monte Carlo realizations by drawing from a multivariate Gaussian distribution. For each realization we compute the relevant ratio(s) and infer Ω_M^Λ (analytically for R_{HH} via Eq. 7, and numerically for R_{HM} and R_{HV}). This procedure automatically propagates all published correlations among the BAO distance measurements into the derived ratios and Ω_M^Λ constraints.

We summarize each derived quantity by the median and central equal-tailed confidence intervals: the 68% CL is given by the 16th and 84th percentiles, and the 95% CL by the 2.5th and 97.5th percentiles.

3. RESULTS

Figure 1 summarizes the BAO distance measurements and the derived null-test constraints on the effective flat- Λ CDM matter density parameter Ω_M^Λ for DESI DR1 and DR2. The corresponding numerical values are listed in Tables 1 and 2. Unless stated otherwise, uncertainties quoted in the tables correspond to central equal-tailed 68% confidence intervals (the 95% intervals are defined analogously; see Sec. 2.6).

3.1. Distance measurements and effective redshift ranges

Panels (A_1) and (B_1) of Fig. 1 compare the directly measured radial BAO distance D_H/r_d (red points) with effective D_H/r_d ranges converted from transverse D_M/r_d and isotropic D_V/r_d measurements (blue and green bands). The converted constraints are displayed as bands because they correspond to an effective line-of-sight distance averaged over a finite redshift interval rather than a strictly local measurement (Sec. 2.3). Overall, the direct and converted distances exhibit broad consistency with each other and with the survey best-fit Λ CDM curve, providing a basic sanity check of the redshift-matching procedure prior to applying the ratio tests.

3.2. Radial–radial ratios: $D_H(z_i)/D_H(z_j)$

The radial–radial ratio test uses only direct D_H/r_d measurements and is therefore the most direct implementation of our sound-horizon-independent null test. The resulting Ω_M^Λ values are shown in panels (A_2) and (B_2) and listed in the first block of Tables 1–2. For DR1, the inferred Ω_M^Λ values span a wide range across the available redshift pairs, while remaining statistically

consistent with a constant value given current uncertainties. For DR2, the additional redshift coverage leads to more ratio combinations, including one high-redshift pair with a highly asymmetric constraint (Table 2), reflecting the limited constraining power of that specific ratio at current precision.

3.3. Radial–transverse ratios: $D_H(z_i)/D_M(z_i)$

Panels (A_3) and (B_3) show Ω_M^Λ inferred from ratios combining a local distance (D_H) with an integrated distance (D_M). Because D_M integrates D_H over $0 < z' < z$, these constraints probe a redshift interval and are presented as bands spanning the corresponding effective z -range (Sec. 2.3). Compared to the radial-only ratios, the D_H/D_M diagnostic yields a relatively stable set of Ω_M^Λ values across redshift in both DR1 and DR2, with the tightest constraints coming from the mid-redshift bins where D_M/r_d is measured most precisely.

3.4. Radial–isotropic ratios: $D_H(z_i)/D_V(z_j)$

The D_H/D_V ratio combines the local expansion rate with the volume-averaged BAO distance. Given the current set of available D_V measurements, the number of independent D_H/D_V ratios is limited (Tables 1–2), and the corresponding Ω_M^Λ constraints remain comparatively weak. Nevertheless, the derived values provide an additional cross-check that mixes radial and isotropic BAO information in a manner that remains independent of the absolute BAO scale.

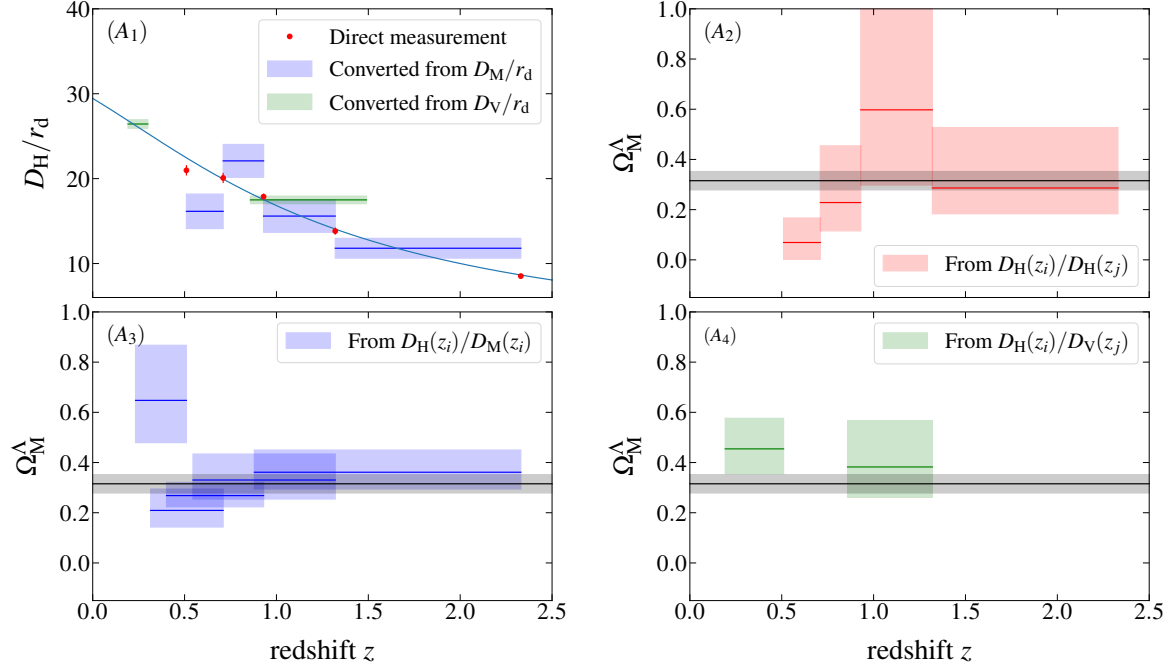
3.5. Summary and DR1–DR2 comparison

To quantify the internal consistency of each diagnostic family, we perform a simple constant- Ω_M^Λ fit within each family and data release. As a descriptive statistic, we treat the entries as independent and use symmetrized 68% uncertainties; this is intended as a compact summary rather than a full likelihood analysis (which would require the complete covariance of the derived ratios). With this convention, the best-fit constants are approximately: $\Omega_M^\Lambda \simeq 0.146$ for the DR1 D_H/D_H ratios and $\Omega_M^\Lambda \simeq 0.214$ for DR2, with $\chi^2/\text{dof} \simeq 1.14$ in both cases; for the D_H/D_M ratios we obtain $\Omega_M^\Lambda \simeq 0.293$ for both DR1 and DR2, with $\chi^2/\text{dof} \simeq 1.45$ (DR1) and $\chi^2/\text{dof} \simeq 1.01$ (DR2). Within the current precision, these fits show no compelling evidence for redshift evolution *within* each diagnostic family, while the differences *between* diagnostic families motivate the discussion in Sec. 4.

4. CONCLUSION

We have presented a simple BAO-based null test of spatially flat Λ CDM built from ratios of BAO distance

From DESI DR1 BAO measurements



From DESI DR2 BAO measurements

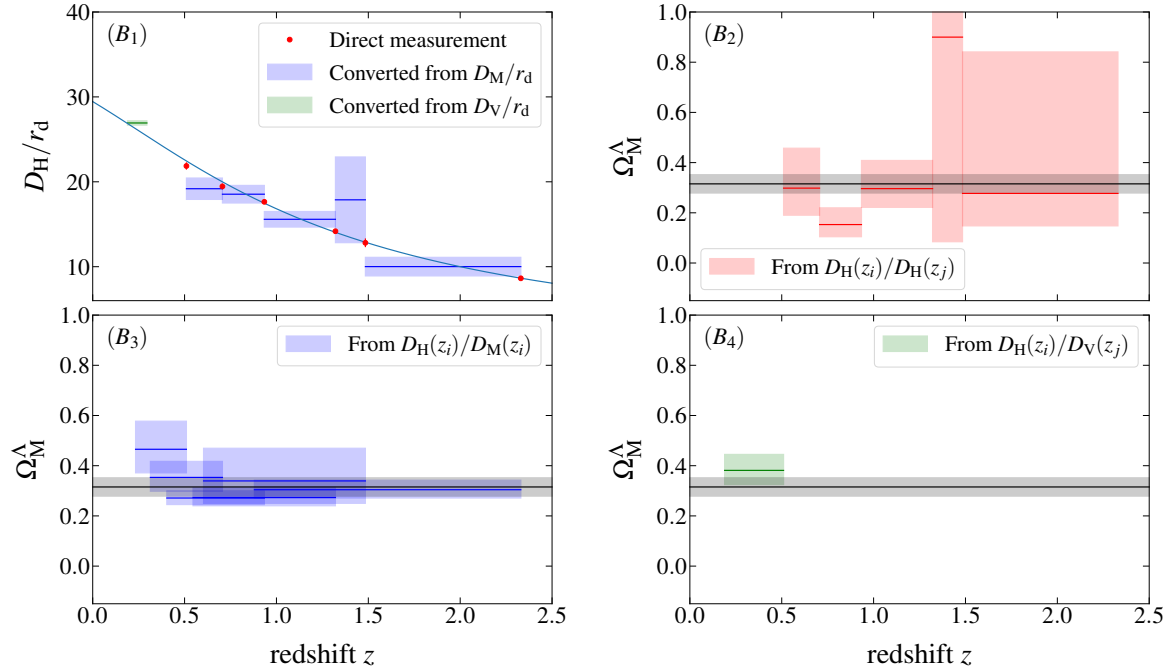


Figure 1. Summary of BAO distances and ratio-based Ω_M^Λ null tests. Panel (A₁): D_H/r_d as a function of redshift for DESI DR1, including direct radial BAO measurements (red points), and the effective D_H/r_d ranges converted from D_M/r_d (blue bands) and D_V/r_d (green bands) using the redshift-matching procedure described in Secs. 2.3–2.4. Panel (A₂): Ω_M^Λ inferred from the radial–radial ratio $D_H(z_i)/D_H(z_j)$ (red bands). Panel (A₃): Ω_M^Λ inferred from the radial–transverse ratio $D_H(z_i)/D_M(z_i)$ (blue bands). Panel (A₄): Ω_M^Λ inferred from the radial–isotropic ratio $D_H(z_i)/D_V(z_j)$ (green bands). Panels (B₁)–(B₄) show the corresponding results for DESI DR2. The gray band in panels (A₂)–(A₄) shows the Planck 2018 flat- Λ CDM constraint on Ω_M (shown for comparison; 68% CL) (P. Collaboration et al. 2020).

$D_{\text{H}}(z_i)/D_{\text{H}}(z_j)$				$D_{\text{H}}(z_i)/D_{\text{M}}(z_i)$			$D_{\text{H}}(z_i)/D_{\text{V}}(z_j)$			
z_i	z_j	$\Omega_{\text{M}}^{\Lambda}$	z -range	z_i	$\Omega_{\text{M}}^{\Lambda}$	z -range	z_i	z_j	$\Omega_{\text{M}}^{\Lambda}$	z -range
0.510	0.710	$0.069^{+0.098}_{-0.067}$	[0.510, 0.710]	0.510	$0.648^{+0.219}_{-0.168}$	[0.233, 0.510]	0.510	0.300	$0.454^{+0.122}_{-0.099}$	[0.192, 0.510]
0.710	0.930	$0.228^{+0.226}_{-0.113}$	[0.710, 0.930]	0.710	$0.209^{+0.085}_{-0.066}$	[0.316, 0.710]	1.320	1.490	$0.382^{+0.185}_{-0.121}$	[0.858, 1.320]
0.930	1.320	$0.598^{+0.402}_{-0.300}$	[0.930, 1.320]	0.930	$0.268^{+0.053}_{-0.044}$	[0.402, 0.930]	-	-	-	-
1.320	2.330	$0.286^{+0.241}_{-0.103}$	[1.320, 2.330]	1.320	$0.330^{+0.104}_{-0.076}$	[0.546, 1.320]	-	-	-	-
-	-	-	-	2.330	$0.361^{+0.088}_{-0.067}$	[0.880, 2.330]	-	-	-	-

Table 1. $\Omega_{\text{M}}^{\Lambda}$ derived from DESI DR1 BAO measurements. We report $\Omega_{\text{M}}^{\Lambda}$ inferred from three ratio tests: radial–radial $D_{\text{H}}(z_i)/D_{\text{H}}(z_j)$, radial–transverse $D_{\text{H}}(z_i)/D_{\text{M}}(z_i)$, and radial–isotropic $D_{\text{H}}(z_i)/D_{\text{V}}(z_j)$. For ratios involving integrated distances, the quoted z -range indicates the effective redshift interval probed by the corresponding measurement (Sec. 2.3). Uncertainties are 68% confidence intervals (Sec. 2.6).

$D_{\text{H}}(z_i)/D_{\text{H}}(z_j)$				$D_{\text{H}}(z_i)/D_{\text{M}}(z_i)$			$D_{\text{H}}(z_i)/D_{\text{V}}(z_j)$			
z_i	z_j	$\Omega_{\text{M}}^{\Lambda}$	z -range	z_i	$\Omega_{\text{M}}^{\Lambda}$	z -range	z_i	z_j	$\Omega_{\text{M}}^{\Lambda}$	z -range
0.510	0.706	$0.298^{+0.159}_{-0.108}$	[0.510, 0.706]	0.510	$0.465^{+0.112}_{-0.094}$	[0.233, 0.510]	0.510	0.295	$0.381^{+0.064}_{-0.057}$	[0.189, 0.510]
0.706	0.934	$0.153^{+0.067}_{-0.049}$	[0.706, 0.934]	0.706	$0.353^{+0.064}_{-0.055}$	[0.314, 0.706]	-	-	-	-
0.934	1.321	$0.296^{+0.112}_{-0.075}$	[0.934, 1.321]	0.934	$0.271^{+0.028}_{-0.026}$	[0.403, 0.934]	-	-	-	-
1.321	1.484	$0.900^{+0.100}_{-0.815}$	[1.321, 1.484]	1.321	$0.273^{+0.039}_{-0.033}$	[0.546, 1.321]	-	-	-	-
1.484	2.330	$0.277^{+0.564}_{-0.129}$	[1.484, 2.330]	1.484	$0.339^{+0.131}_{-0.089}$	[0.603, 1.484]	-	-	-	-
-	-	-	-	2.330	$0.304^{+0.038}_{-0.033}$	[0.880, 2.330]	-	-	-	-

Table 2. Same as Table 1 but for DESI DR2 BAO measurements.

measurements. The central idea is to map each observed ratio to an *effective* flat- Λ CDM matter density parameter, Ω_M^Λ , defined as the value of Ω_M for which the corresponding Λ CDM prediction reproduces the measured ratio. Because BAO constraints are typically reported in units of the sound horizon, and because our diagnostics use ratios of BAO distances, the dependence on the absolute BAO scale r_d cancels identically; moreover, the overall normalization set by H_0 drops out of the ratios. This yields a transparent, calibration-free internal consistency check that can combine radial and transverse BAO information within a single framework.

We applied the test to BAO measurements from the DESI Data Release 1 and Data Release 2 (A. G. Adame et al. 2025a; M. Abdul Karim et al. 2025), using three complementary families of ratios: a purely radial test based on $D_H(z_i)/D_H(z_j)$, and two mixed tests combining D_H with the integrated distances D_M and D_V . For transverse and isotropic BAO, we adopted a redshift-matching strategy based on the integral mean value theorem to associate integrated distances with an effective line-of-sight distance over a well-defined redshift interval. All inferred ratios and Ω_M^Λ constraints were obtained by propagating the *full* DESI BAO covariance matrices through Monte Carlo sampling. Within current uncertainties, the inferred Ω_M^Λ values are broadly consistent with a redshift-independent constant, and hence with the flat- Λ CDM expectation. Mild deviations appear for some redshift ranges in the mixed D_H/D_M and D_H/D_V diagnostics, but these are not statistically significant at the present precision.

Interpreted as a null test, any statistically significant redshift dependence of Ω_M^Λ *within* a given diagnostic family, or a robust inconsistency *between* different families constructed from the same dataset, would signal a departure from flat Λ CDM. Such a failure could arise from dynamical dark energy, spatial curvature, modified gravity, or residual observational systematics, and would therefore motivate further investigation rather than a unique physical interpretation. The ratio-based nature of the test makes it particularly useful for tracking internal consistency as BAO measurements improve.

Looking ahead, future DESI data releases, together with forthcoming wide-area surveys—including the Subaru Prime Focus Spectrograph (PFS) (M. Takada et al. 2014), ESA’s *Euclid* mission (R. Laureijs et al. 2011), and the Nancy Grace Roman Space Telescope (D. Spergel et al. 2015; R. Akeson et al. 2019)—will provide more precise distance measurements over wider redshift ranges, enabling substantially more stringent tests of the constancy of Ω_M^Λ and allowing finer redshift binning and a larger set of ratio combinations. The same framework

can also be generalized to additional background models (e.g. including curvature or simple w CDM extensions), and can be combined with independent late-time probes to help diagnose the origin of any detected inconsistencies.

ACKNOWLEDGEMENTS

We thank Gong-Bo Zhao for insightful discussions. This work is supported by National Key R&D Program of China (grant no. 2023YFA1605600), National Natural Science Foundation of China (#12525303), and Tsinghua University Initiative Scientific Research Program.

DATA AVAILABILITY

The BAO measurements used in this work are taken from the DESI public data releases (A. G. Adame et al. 2025a; M. Abdul Karim et al. 2025). The analysis code (written in Julia) used to produce the results and figures is available at https://github.com/adamcosmology/newOm_BAO/.

APPENDIX

A. DISTANCE MAPPING FOR D_M AND D_V

Transverse and isotropic BAO distances encode *integrated* information about the local Hubble distance $D_H(z) \equiv c/H(z)$. For the purposes of interpretation and for quoting the redshift intervals probed by ratios involving D_M or D_V , it is useful to associate these integrated distances with an “effective” line-of-sight distance at a lower redshift.

A.1. *Mapping $D_M(z)$ to an effective $D_H(z_c)$*

By definition,

$$D_M(z) = \int_0^z D_H(z') dz'. \quad (\text{A1})$$

Since $D_H(z)$ is continuous in any standard cosmological model, the integral mean value theorem (W. Rudin 1976) guarantees the existence of an intermediate redshift $z_c \in (0, z)$ such that

$$D_M(z) = z D_H(z_c) \iff D_H(z_c) = \frac{D_M(z)}{z}. \quad (\text{A2})$$

In a given background model (e.g. flat Λ CDM specified by Ω_M), the mapping $z \mapsto z_c(z)$ can be obtained by numerically solving $D_H(z_c) = D_M(z)/z$.

A.2. *Mapping $D_V(z)$ to an effective $D_H(z_d)$*

The isotropic BAO distance is

$$D_V(z) = [z D_M^2(z) D_H(z)]^{1/3}. \quad (\text{A3})$$

Combining this with $D_M(z) = z D_H(z_c)$ yields

$$D_V(z) = z [D_H^2(z_c) D_H(z)]^{1/3} \equiv z D_H(z_d), \quad (\text{A4})$$

for some z_d that satisfies $z_c < z_d < z$ (W. Rudin 1976). Equivalently,

$$D_H(z_d) = \frac{D_V(z)}{z}, \quad z_d \in (z_c, z), \quad (\text{A5})$$

and, for a specified background model, z_d is obtained by numerically solving the above equation.

A.3. *Conservative bracketing and the quoted z -ranges*

The intermediate redshifts z_c and z_d are not directly observable, and the mapping depends (weakly) on the background model through $D_H(z)$. In this work we use these mappings only to provide a transparent *redshift range* for ratios involving integrated distances (see Sec. 2.3). In flat Λ CDM, both $z_c(z)$ and $z_d(z)$ decrease monotonically as Ω_M increases; therefore, choosing $\Omega_M = 1$ yields a conservative *lower bound* on the effective redshift associated with a given $D_M(z)$ or $D_V(z)$. To bracket the mapping, we scan Ω_M over a broad prior $\Omega_M \in [0, 1]$ and report the corresponding range of z_c (or z_d) when quoting the z -interval probed by D_H/D_M and D_H/D_V ratios.

Figure 2 illustrates the mapping between the redshift at which D_M or D_V is measured and the effective redshift at which a local D_H reproduces $D_M(z)/z$ or $D_V(z)/z$ in flat Λ CDM for representative values of Ω_M .

REFERENCES

Abdul Karim, M., et al. 2025, Phys. Rev. D, 112, 083515, doi: 10.1103/tr6y-kpc6	Adame, A. G., et al. 2025b, JCAP, 01, 124, doi: 10.1088/1475-7516/2025/01/124
Adame, A. G., et al. 2025a, JCAP, 04, 012, doi: 10.1088/1475-7516/2025/04/012	Akeson, R., et al. 2019, arXiv e-prints, doi: 10.48550/arXiv.1902.05569

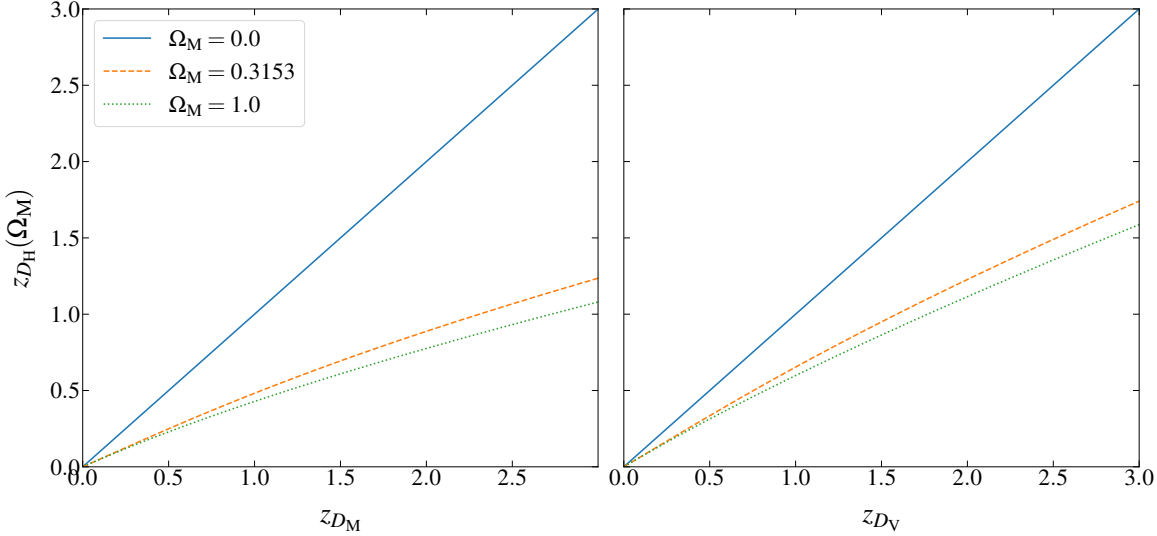


Figure 2. Effective-redshift mapping implied by $D_M(z) = z D_H(z_c)$ (left) and $D_V(z) = z D_H(z_d)$ (right) in flat Λ CDM for representative values of Ω_M . For each z , the mapped redshifts satisfy $0 < z_c < z_d < z$. Increasing Ω_M shifts both z_c and z_d to lower values, so $\Omega_M = 1$ provides a conservative lower bound for the effective redshift associated with a given $D_M(z)$ or $D_V(z)$.

Alam, S., Aubert, M., Avila, S., et al. 2021, Physical Review D, 103, 083533, doi: [10.1103/PhysRevD.103.083533](https://doi.org/10.1103/PhysRevD.103.083533)

Bennett, C. L., Banday, A. J., Górski, K. M., et al. 1996, Astrophysical Journal Letters, 464, L1, doi: [10.1086/310075](https://doi.org/10.1086/310075)

Caldwell, R. R., Dave, R., & Steinhardt, P. J. 1998, Physical Review Letters, 80, 1582, doi: [10.1103/PhysRevLett.80.1582](https://doi.org/10.1103/PhysRevLett.80.1582)

Carroll, S. M. 2001, Living Reviews in Relativity, 4, 1, doi: [10.12942/lrr-2001-1](https://doi.org/10.12942/lrr-2001-1)

Cole, S., Percival, W. J., Peacock, J. A., et al. 2005, Monthly Notices of the Royal Astronomical Society, 362, 505, doi: [10.1111/j.1365-2966.2005.09318.x](https://doi.org/10.1111/j.1365-2966.2005.09318.x)

Collaboration, P., Aghanim, N., Akrami, Y., Ashdown, M., et al. 2020, Astronomy & Astrophysics, 641, A6, doi: [10.1051/0004-6361/201833910](https://doi.org/10.1051/0004-6361/201833910)

de Bernardis, P., Ade, P., Bock, J., et al. 2000, Nature, 404, 955, doi: [10.1038/35010035](https://doi.org/10.1038/35010035)

Eisenstein, D. J., Zehavi, I., Hogg, D. W., et al. 2005, The Astrophysical Journal, 633, 560, doi: [10.1086/466512](https://doi.org/10.1086/466512)

Halverson, N. W., Leitch, E. M., Pryke, C., et al. 2002, Astrophysical Journal, 568, 38, doi: [10.1086/338879](https://doi.org/10.1086/338879)

Laureijs, R., Amiaux, J., Arduini, S., et al. 2011, arXiv e-prints, doi: [10.48550/arXiv.1110.3193](https://doi.org/10.48550/arXiv.1110.3193)

Peebles, P. J. E. 1980, The Large-Scale Structure of the Universe (Princeton, NJ: Princeton University Press)

Perlmutter, S., Aldering, G., Goldhaber, G., et al. 1999, The Astrophysical Journal, 517, 565, doi: [10.1086/307221](https://doi.org/10.1086/307221)

Ratra, B., & Peebles, P. J. E. 1988, Physical Review D, 37, 3406, doi: [10.1103/PhysRevD.37.3406](https://doi.org/10.1103/PhysRevD.37.3406)

Riess, A. G., Filippenko, A. V., Challis, P., et al. 1998, The Astronomical Journal, 116, 1009, doi: [10.1086/300499](https://doi.org/10.1086/300499)

Rudin, W. 1976, Principles of Mathematical Analysis, 3rd edn. (New York: McGraw-Hill)

Sahni, V., Shafieloo, A., & Starobinsky, A. A. 2008, Physical Review D, 78, 103502, doi: [10.1103/PhysRevD.78.103502](https://doi.org/10.1103/PhysRevD.78.103502)

Sahni, V., Shafieloo, A., & Starobinsky, A. A. 2014, The Astrophysical Journal, 793, L40, doi: [10.1088/2041-8205/793/2/L40](https://doi.org/10.1088/2041-8205/793/2/L40)

Shafieloo, A., Sahni, V., & Starobinsky, A. A. 2012, Physical Review D, 86, 103527, doi: [10.1103/PhysRevD.86.103527](https://doi.org/10.1103/PhysRevD.86.103527)

Smoot, G. F., Bennett, C. L., Kogut, A., Wright, E. L., et al. 1992, Astrophysical Journal Letters, 396, L1, doi: [10.1086/186504](https://doi.org/10.1086/186504)

Spergel, D., Gehrels, N., Baltay, C., et al. 2015, arXiv e-prints, doi: [10.48550/arXiv.1503.03757](https://doi.org/10.48550/arXiv.1503.03757)

Takada, M., et al. 2014, Publications of the Astronomical Society of Japan, 66, R1, doi: [10.1093/pasj/pst019](https://doi.org/10.1093/pasj/pst019)

Weinberg, S. 1989, Reviews of Modern Physics, 61, 1, doi: [10.1103/RevModPhys.61.1](https://doi.org/10.1103/RevModPhys.61.1)

Zunckel, C., & Clarkson, C. 2008, Physical Review Letters, 101, 181301, doi: [10.1103/PhysRevLett.101.181301](https://doi.org/10.1103/PhysRevLett.101.181301)